J Solid State Electrochem (2008) 12:1337–1348
DOI 10.1007/s10008-008-0542-2

ORIGINAL PAPER

The influence of edge-plane defects and oxygen-containing surface groups on the voltammetry of acid-treated, annealed and "super-annealed" multiwalled carbon nanotubes

Andrew F. Holloway · Gregory G. Wildgoose · Richard G. Compton · Lidong Shao · Malcolm L. H. Green

Received: 4 February 2008 / Accepted: 4 March 2008 / Published online: 14 May 2008

Abstract The role of edge-plane-like defects at the open ends of multiwalled carbon nanotubes (MWCNTs) and at hole defects in the tube walls is explored using cyclic voltammetry with two charged redox probes, namely potassium ferrocyanide and hexaaminеruthenium(III) chloride in unbuffered aqueous solutions, and one neutral redox probe, norepinephrine, in pH 5.7 buffer. Further, the presence of oxygen-containing functional groups (such as phenol, quinonyl and carboxyl groups), which decorate the edge-plane defect sites on the voltammetric response of the MWCNTs, is also explored. To this end, three different pre-treatments were performed on the pristine MWCNTs made using the arc-discharge method (arc-MWCNTs). These were (a) arc-MWCNTs were subjected to acid oxidation to form acid-MWCNTs—open-ended MWCNTs also possessing numerous hole defects revealing a large number of edge-plane-like sites heavily decorated with surface functional groups; (b) acid-MWCNTs, which were subsequently vacuum-annealed at 900 °C to remove the functional groups but leaving the many undecorated edge-plane-like sites exposed (ann-MWCNTs); (c) ann-MWCNTs, which were subjected to a further vacuum "super-annealing" stage at 1,750 °C (sup-MWCNTs), which caused the hole defects to close and also closed the tube ends, thereby, restoring the original, pristine, almost edge-plane defect-free MWCNTs structure. The results of the voltammetric characterisation of the acid-, ann- and sup-MWCNTs provide further evidence that edge-plane-like sites are the electroactive sites on MWCNTs. The presence of oxygen-containing surface groups is found to inhibit the rate of electron transfer at these sites under the conditions used herein. Finally, the two charged, "standard" redox probes used were found to undergo strong interactions with the oxygen-containing surface groups present. Thus, we advise caution when using these redox probes to attempt to voltammetrically characterise MWCNTs, and by extension, graphitic carbon surfaces.

Keywords Multiwalled carbon nanotubes · Edge-plane defects · Surface groups · Acid pre-treatment · Voltammetry

Introduction

Multiwalled carbon nanotubes (MWCNTs) were arguably first discovered [1] in 1976 by Oberlin and Endo [2] and separately in 1978 by Wiles and Abrahamson [3] before being sensationally rediscovered in 1991 by Iijima [4]. Structurally, they can be considered to be seamlessly "rolled up" sheets of graphene, with concentric tubes stacked one inside the other. Typically, MWCNTs are several tens of nanometres in diameter and have lengths of the order of several microns. Within this general structure, several morphological variations exist, such as "hollow-tube", "herringbone" or "bamboo-like" MWCNTs. In the

A. F. Holloway · G. G. Wildgoose (✉) · R. G. Compton
Department of Chemistry,
Physical and Theoretical Chemistry Laboratory,
University of Oxford,
South Parks Road,
Oxford OX1 3QZ, UK
e-mail: gregory.wildgoose@chem.ox.ac.uk

L. Shao · M. L. H. Green
Department of Chemistry, Inorganic Chemistry Laboratory,
University of Oxford,
South Parks Road,
Oxford OX1 3QR, UK

first two morphologies, the tubes remain open along their entire length, with the graphite sheets forming the tube walls either parallel to the MWCNT axis in the case of hollow-tube or offset at a slight angle to the axis of the tube in the case of herringbone. Bamboo-like MWCNTs have a similar internal structure to the herringbone MWCNTs except that the tubes are periodically closed off into compartments, rather like the structure of the bamboo plant from which they take their name [5].

The different morphologies of the MWCNTs depend strongly upon the method and conditions used during their manufacture [6]. Two principle methods of forming MWCNTs exist. The first is chemical vapour deposition, which involves the decomposition of various hydrocarbon gases at elevated temperatures over metal nanoparticle "seed" catalysts supported on an appropriate surface such as an iron plate [7, 8]. Depending on the temperature, any of the three main morphologies of MWCNT can be produced. The second method is the arc-discharge method [9–11] described in more detail in "Synthesis and preparation of arc-MWCNTs, acid pre-treated, annealed and super-annealed MWCNTs" below. This method predominantly produces hollow-tube MWCNTs, the type used herein, usually with high purity (and largely free from the amorphous carbon deposits commonly found in cvd-MWCNTs), with the ends of the MWCNTs closed by fullerene-like caps. One advantage of the arc-discharge method is that the method can be used without the need for metal nanoparticle catalysts whose persistent and residual presence within the MWCNTs can provide electroactive sites for certain analytes to which the MWCNTs are otherwise inert, resulting in potentially misleading interpretation of the voltammetric results [12–18].

Unlike their single-walled analogues where some ambiguity still remains, much is now understood about the underlying causes of much of the voltammetry observed at MWCNT-modified electrodes. By analogy to the structure of graphite, the tube ends have similar properties to the edge-plane face of a graphite crystal, whilst the tube walls can be described as "basal-plane" like by analogy to the other crystal face of graphite (the plane containing all the carbon atoms of one sheet of graphene, which is perpendicular to the edge-plane crystal faces) [19–21]. Compared to a well-prepared edge-plane pyrolytic graphite electrode (eppg), it is suggested that the electroactive sites on the MWCNTs are situated at edge-plane-like sites at the ends of the tubes and at defects (holes) in the tube walls [19–21]. The walls of the tubes are considered to be more basal-plane like in that the rate of electron transfer at the tube walls is so slow compared to the tube ends as to be negligible or zero. In fact, for most electroanalytical applications, it has been shown that eppg electrodes are in fact the optimal electrode of choice compared to MWCNT-modified electrodes [20].

The edge-plane-like sites on the surface of the MWCNTs are known to be decorated with oxygen-containing functional groups, in particular, hydroxyl/phenol, quinonyl and carboxyl groups are almost always present [22–24] (for a more detailed review, see references contained in [23]). The role that these surface functional groups play in facilitating or hindering electron transfer to various redox species in solution remains rather unclear. Some reports claim that under certain specific conditions, redox catalysis by oxo-surface groups such as, for example, quinonyl groups on the surface, can enhance the rate of electron transfer in certain cases [25–31]. There is, however, some evidence from this laboratory that the converse is true and that the presence of other oxygenated species (e.g. carboxyl, phenols and lactones) on eppg and MWCNT electrodes can actually inhibit the rate of electron transfer [32, 33].

This paper seeks to resolve this question and to attempt to complete our understanding of the part these surface groups play and to explore the electron transfer at pure edge-plane-like defects on the surface of the MWCNTs. To this end, arc-MWCNTs, which are free from any metal catalyst impurities, are synthesised and subjected to an oxidative acid pre-treatment commonly used in the literature [31, 34]. This pre-treatment has the effect of both opening the arc-MWCNTs (which are formed with closed ends) and attacking the pristine tube walls to introduce holes (and hence edge-plane-like defects in the MWCNT structure) and decorating the edge-plane-like defects with oxygen-containing groups. Such pre-treatments are commonly used in the literature to increase the number of synthetically useful carboxyl groups on the nanotube surface. However, it has been shown that whilst the overall number of carboxyl groups does increase with pre-treatment, the number of quinone groups on the surface can also increase to a greater extent [23]. The acid pre-treated arc-MWCNTs will subsequently be denoted as acid-MWCNTs. Next, the acid-MWCNTs are annealed under vacuum at 900 °C, which removes any oxygen-containing surface groups to leave the tube ends and hole defects exposing bare, undecorated edge-plane-like defect sites. These are labelled as ann-MWCNTs. Finally, the hole defects and tube ends are closed to restore the pristine structure of the ann-MWCNTs by "super-annealing" under vacuum at 1,750 °C, denoted as "sup-MWCNTs". Each material was characterised using high-resolution transmission electron microscopy (HRTEM), Fourier transform infra red spectroscopy (FTIR) and Raman spectroscopy. The voltammetric responses of the acid-, ann- and sup-MWCNTs towards two common redox probes, namely ferrocyanide $\left(Fe(CN)_6^{4-}\right)$ and hexaaminеruthenium(III) $\left(Ru(NH_3)_6^{3+}\right)$ in unbuffered electrolyte, and the neutral species norepinephrine in pH 5.7 buffer was recorded. This then allows us to compare each type of defect site, namely decorated edge-plane vs. undecorated

edge-plane vs. almost no edge-plane sites, and to elucidate the role that both oxygen-containing surface groups and edge-plane defect sites play during electron transfer.

Materials and methods

Reagents and equipment

All reagents were purchased from Aldrich (Gillingham, UK) and were of the highest commercially available grade and used without further purification. Aqueous solutions were prepared using UHQ deionised water from a Millipore (Vivendi, UK) UHQ grade water system, with a resistivity of not less than 18.2 MΩ cm at 298 K.

Cyclic voltammetry was performed on a μAutolab type III computer-controlled potentiostat (EcoChemie, Utrecht, Netherlands) using a standard three-electrode configuration. A bright platinum wire served as the counter electrode in conjunction with a saturated calomel reference electrode (SCE, Radiometer, Copenhagen, Denmark). The cell assembly was completed using either a glassy carbon electrode (GC; BAS Technicol, USA, diameter 3 mm), an edge-plane electrode (eppg, Le Carbone, Sussex, UK, diameter 5 mm) or a basal-plane electrode (bppg; Le Carbone, Sussex, UK, diameter 5 mm) as the working substrate electrode. The bppg electrode surface was renewed by pressing the surface onto cello tape and removing the top few layers of graphite. This was repeated several times, and finally, the electrode surface was rinsed in acetone to remove any residual adhesive from the cello tape. The eppg electrode was successively polished using alumina slurry (Beuhler, USA, 3.0 μm–0.1 μm) and sonicated after each polishing to remove any adhered microparticles of alumina. All electrolyte solutions were degassed with pure argon (BOC gases, Guildford, UK) for 30 min prior to commencing any voltammetric measurements.

HRTEM was performed using a JEOL 4000EX microscope and energy dispersive X-ray (EDX) analysis using a JEOL 2010 microscope on an Oxford Instruments LZ5 windowless detector controlled by INCA software. The samples were ground and dispersed in ethanol and then placed drop wise onto a holey carbon support grid.

FTIR spectra were recorded in transmission mode on a Nicolet MAGNA-IR 560 spectrometer at 4-cm^{-1} resolution by co-adding 128 scans (MCT/B detector; CsI beam splitter; Happ-Genzel apodisation). Thin films of the carbon nanotube samples were prepared on ZnSe disks (2-mm thickness) by dropping a suspension of nanotubes in 2-propanol onto the preheated substrates (70 °C). Film thicknesses were increased until the absorbance of the background was ~1. Spectra were then corrected so that the lowest point of the background equals 1.

Raman spectra were recorded on a Jobin Yvon spectrometer (Labram 1B) equipped with a microscope through a 50-fold magnification objective (Olympus Co.) by adding four sets of spectra together. A 20-mW He–Ne laser (632 nm) was used. The 1,800 lines per millimetre grating provides a resolution starting from 1.0 cm^{-1} at 200 cm^{-1} up to 0.5 cm^{-1} at 3,600 cm^{-1}. The abscissa was calibrated with a silicon standard, and the sharp Raman shifts are accurate to ±2 cm^{-1}. Raman spectra were directly taken from the thin films prepared for IR spectroscopy. To ensure homogeneity of the samples, three spectra were recorded from different spots on the sample (laser spot diameter ~1 μm). The Raman spectra were baseline-corrected.

Synthesis and preparation of arc-MWCNTs, acid pre-treated, annealed and super-annealed MWCNTs

The native arc-MWCNTs were made in house following the standard Kratschmer–Huffman type electric arc synthesis [9, 10]. This metal nanoparticle catalyst-free method involves the vaporisation of a graphite anode by an electric arc inside a chamber, filled with a reduced pressure of helium gas. The use of a pure graphite rod as the anode results in the formation of a hard deposit on the cathode, the soft core of which contains the arc-MWCNTs. This method of producing arc-MWCNTs also results in the formation of some nanometer-sized polyhedral "onions", which have similar physical and chemical properties as the arc-MWCNTs themselves, and as such, can never be completely removed from the MWCNTs amongst which they are distributed [35]. The contribution of these structures, some of which also possess edge-plane-like defects, on the voltammetric response of this material has been described elsewhere [35] and will be discussed where necessary herein.

Oxidative acid pre-treatment of the arc-MWCNTs was performed using a method adapted from the work of Smalley et al. [36] by suspending a 20-mg sample of the arc-MWCNTs in 40 mL of a 3:1 mixture of concentrated H_2SO_4/HNO_3 and refluxed at 110 °C for 4 h. The resultant suspension was allowed to cool, carefully diluted with 200 mL of pure water and finally filtered under suction. The resulting acid pre-treated MWCNTs (acid-MWCNTs) were then dried at 100 °C overnight before being stored in an airtight container prior to use.

In order to remove any oxygen-containing functional groups from the edge-plane-like defects introduced during the acid pre-treatment step, the acid pre-treated MWCNTs were annealed at 900 °C under a vacuum of no greater than 10^{-5} Torr for 2 h, which has been shown to be sufficient to remove all oxygen-containing functionality from the surface of the nanotubes [37]. These annealed MWCNTs (ann-MWCNTs) were then stored under vacuum, sealed in a quartz ampoule prior to first use, and then stored

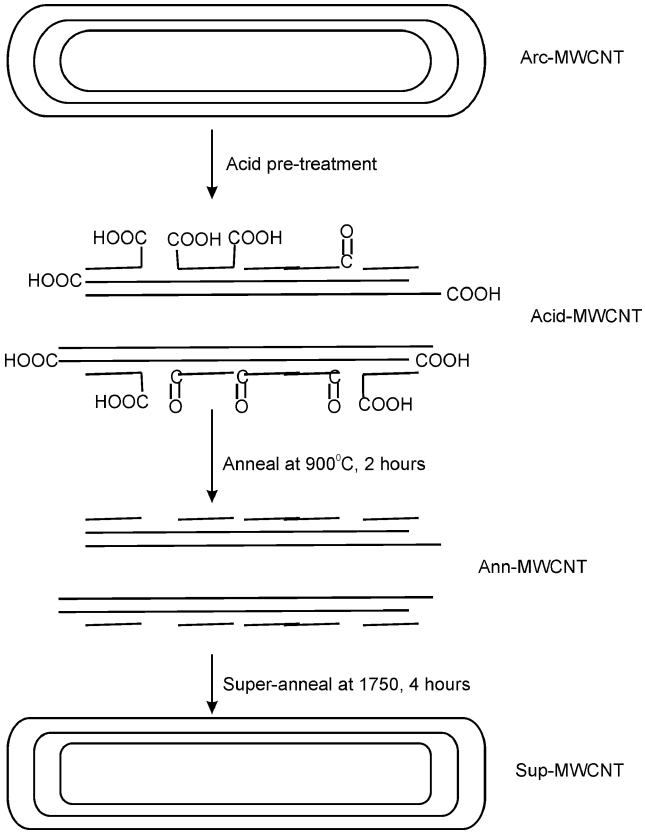

Scheme 1 A schematic cross-sectional representation of the consecutive formation and principal structural features of the arc-, acid-, ann- and sup-MWCNTs

in an airtight container under an inert, oxygen-free argon atmosphere.

Finally, in order to reconstruct the pristine MWCNT structure, a sample of the annealed MWCNTs was subject to a further super-annealing step. This involved heating a sample of the annealed MWCNTs to 1,750 °C, again under a vacuum of at least 10^{-5} Torr for a period of 4 h. This has been shown to reconstruct and restore the pristine structure of the nanotubes [38, 39], closing any defects (holes) in the tube walls and resulting in the formation of closed-ended sup-MWCNTs possessing little or no edge-plane defect sites. The sup-MWCNTs were stored in an airtight container prior to use. Each step of this process is illustrated in Scheme 1.

Immobilisation of the MWCNTs onto the working electrode substrate

To immobilise the MWCNTs onto the working electrode, a casting suspension (1 mg/mL) was made up in chloroform with 30-min sonication. The GC working electrode was first polished using successive grades of diamond lapping spray (Kemet, UK) from 6.0- to 0.1-μm particle size. After each successive polishing, the electrode was sonicated briefly and rinsed in ethanol to remove any adhered microparticles. Finally, a 20 μL aliquot of the appropriate casting suspension was placed onto the electrode surface, and the solvent was then allowed to evaporate at room temperature, leaving the MWCNTs immobilised onto the electrode surface.

Results and discussion

Microscopic and vibrational spectroscopic characterisation

The characterisation of the arc-MWCNTs has been described elsewhere [35] and produced closed-ended MWCNTs, 20± 10 nm in diameter and several microns in length. The acid-MWCNTs were first characterised using HRTEM. Figure 1 shows acid-treated MWCNTs, which are 20±10 nm in diameter and several microns in length similar to the untreated arc-MWCNTs. It can be see that the pristine structure of the arc-MWCNTs has been severely damaged; the acid-MWCNTs are now open-ended, whilst numerous holes and defects can be seen along the walls of the nanotubes. The ann-MWCNTs (not shown) were found to be almost identical in structure to the acid-MWCNTs, showing that the removal of the oxygen-containing surface groups has not changed the observable structure at the resolution used. Figure 2 shows HRTEM images of the sup-MWCNTs. It can be seen that the ends of the tubes are now closed, the holes and defects in the tube walls have been removed and that there is very little amorphous carbon coating the tube walls. The structure of the sup-MWCNTs is almost identical to that of the arc-MWCNTs starting material [35].

The baseline-corrected Raman spectra recorded over the region of the D and G bands of the acid-, ann- and sup-MWCNTs are shown in Fig. 3 for comparison. Wider scans were performed, but no spectral peaks of interest were observed apart from the higher order harmonic resonances of the two bands of interest. In all cases, two principal spectral peaks corresponding to the D-band radial breathing mode and the G-band tangential stretching mode are observed at ca. 1,333 cm^{-1} and ca. 1,578 cm^{-1}, respectively, in agreement with the literature [40–46]. Tuinistra and Koenig [47] developed a relationship between the mean crystallite size (the in-plane coherence length, L_a) in graphite and the ratio of intensities of the D and G bands (I_D and I_G, respectively), and this has been extended to all types of CNTs, whereby the ratio of the intensities of the D and G bands relates to the degree of disorder in the CNTs, or more specifically, the extent of side-wall functionalisation [40, 41, 43–46, 48]. A ratio of $I_D/I_G>1$ infers a high degree of disorder and side-wall functionalisation of the CNTs, whilst

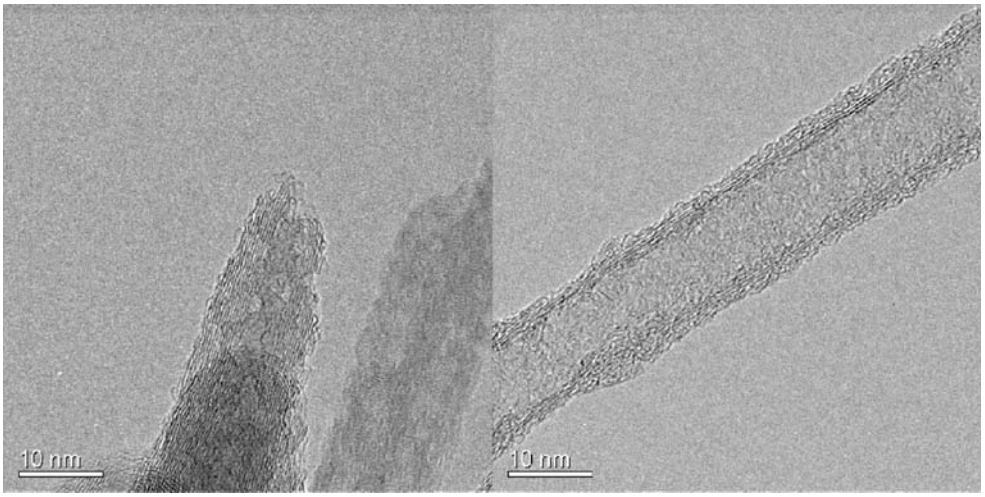

Fig. 1 HRTEM images of the acid-MWCNTs showing the oxidative opening of the tube ends (*left*) and the damage caused to the sidewalls of the acid-MWCNTs

a ratio close to zero indicates a high degree of crystallinity associated with pristine CNTs. Furthermore, any increase in the width of the D band has been attributed to side-wall functionalisation [40, 41, 43–46, 48]. The I_D/I_G ratios and full-height half-widths for each of the MWCNTs studied are given in Table 1. It is clear that the degree of disorder and side-wall functionality (at the holes and defects decorated with oxygen-containing surface groups) has successively decreased between the acid-, ann- and sup-MWCNTs, respectively.

The overlaid FTIR spectra are shown in Fig. 4. In the acid-MWCNT, FTIR spectrum two broad spectral peaks can be observed at ca. 1,620–1,720 and 1,103–1,242 cm^{-1}, which we assign to C=O and C–O stretches from surface quinone and/or carboxyl groups. There may be a broad, ill-defined peak(s) in the range 2,500–3,500 cm^{-1}, which encompasses the region of –OH stretches of both carboxyl and hydroxyl/phenol groups, but it is unclear whether any absorbance in this region is simply the spectral background or whether it is actually due to these functional groups. By comparison to the other spectra, it is possible that this feature is attributable to –OH stretches, but we cannot categorically state this to avoid over interpretation of the data.

In contrast, the ann-MWCNTs do not show any of the spectral features observed in the acid-MWCNT spectra, confirming that the oxygen-containing surface groups have been removed by the annealing process. Two smaller peaks are just observable above the background at 1,373 and 1,605 cm^{-1}, which remain unassigned but may speculatively be due to C–H "rocking" and C–C in-plane stretches, respectively. The sup-MWCNT spectrum shows no clearly defined spectral features, certainly indicating that there are no surface functional groups present.

The results of the HRTEM, Raman and FTIR characterisation are consistent with the proposed structures of each type of MWCNT studied herein.

Voltammetric characterisation of the acid-, ann- and sup-MWCNTs in aqueous electrolyte

First, cyclic voltammetry was performed at the bare GC, eppg and bppg electrodes in two different solutions

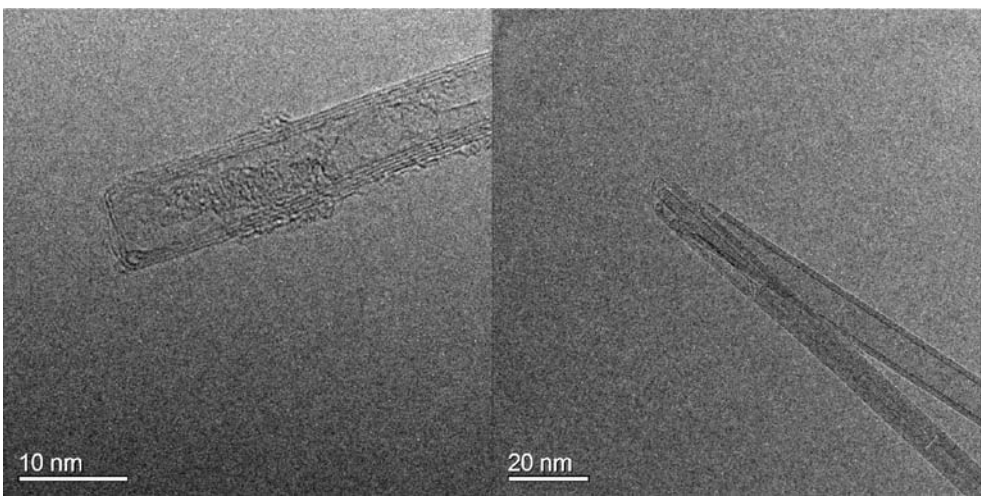

Fig. 2 HRTEM images of the sup-MWCNTs showing the restoration of the pristine structure of the MWCNTs, with little or no defects present along the tube walls (*right*) and the closure of the tube ends (*left*)

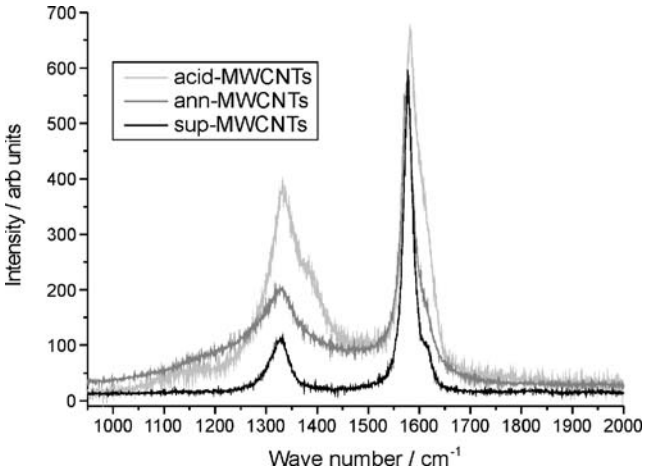

Fig. 3 Overlaid baseline-corrected Raman spectra of the acid-, ann- and sup-MWCNTs scanned from 950–2,000 cm^{-1} over the region of interest containing the D and G bands

containing standard redox probes, either 1.0 mM potassium ferrocyanide or 1.0 mM hexaammineruthenium(III) chloride, with each solution containing 0.1 M potassium chloride as supporting electrolyte. The potential was cycled between −0.2 to 0.5 V in the case of ferrocyanide and 0.2 to −0.5 V for the hexaammineruthenium(III) complex. The potential scan rate was varied in each case over the range 10–500 mV s^{-1}. A single, quasi-reversible set of redox peaks was observed for both the ferrocyanide and the hexaammineruthenium(III) complex centred on mid-peak potentials of 0.19 and −0.185 V, respectively, as expected. Plots of peak current vs. the square root of the voltage scan rate were linear in all cases, indicating that the voltammetry was under diffusion control [49, 50]. The peak-to-peak separation is a measure of the rate of the electron transfer kinetics, with an ideal value of 59 mV for a reversible redox system with fast electron kinetics at 298 K [49, 50]. The peak-to-peak separations (measured at 100 mV s^{-1}) using ferrocyanide were 63, 131 and 223 mV and in hexaammineruthenium were 63, 64 and 282 mV at the bare eppg, GC and bppg electrodes, respectively. It is apparent that the bppg electrode, with the largest peak-to-peak separation, has the most sluggish electrode kinetics due to the relative paucity of edge-plane sites on its surface, whilst the eppg electrode has the fastest rate of electron transfer, and GC is intermediate between the two, as expected from previous studies. It is also apparent that the hexaammineruthenium(III) complex behaves much more like an ideal, one-electron outer-sphere redox probe than the ferrocyanide ion does at carbon electrodes. The behaviour of ferrocyanide at carbon surfaces, and whether it should actually be considered as a standard, outer-sphere redox probe (at least for studies at carbon electrode surfaces) is debatable, as discussed in the "Introduction", and we will return to this issue in light of the MWCNT voltammetry discussed below.

In order to characterise the voltammetry of the MWCNTs and to investigate the effects of oxygen-containing surface groups and edge-plane defect sites on the observed electron transfer kinetics, each of the acid-, ann- and sup-MWCNTs were separately cast onto a GC electrode, and cyclic voltammetry was carried out in the same manner as described above, again in 1.0 mM potassium ferrocyanide or 1.0 mM hexaammineruthenium(III) chloride solutions. Figure 5a and b show the voltammetric responses towards both the ferrocyanide and hexaammineruthenium(III) redox probes obtained at the acid-MWCNT-modified GC electrode. The observed voltammetry is markedly different from that seen at the bare carbon electrodes described above. In the case of ferrocyanide (Fig. 5a), upon scanning in the oxidative direction, a broad oxidative peak is observed at ca 0.2 V vs. SCE, superimposed onto a large capacitive background charging current which is a "typical" feature of nanotube voltammetry—discussed below. However, the wave shape is now more characteristic of a species adsorbing from solution onto a surface rather than a species diffusing in solution [49, 50]. Upon reversing the scan direction, a very sharp reduction wave is observed, which, rather unusually, is almost triangular in shape and whose wave shape is almost more akin to that of a stripping wave than to a diffusion-controlled process, especially at low scan rates. Yet a plot of peak current vs. square root scan rate remains linear (R^2= 0.98) for both the oxidative and reductive peaks, indicating that the voltammetry is still under diffusion control.

To explain this unusual behaviour, we note that the oxidation product is ferricyanide in which the iron(III) centre is in a d^5 low-spin electronic configuration. Ferricyanide, unlike ferrocyanide (d^6, low spin), is known to be reasonably

Table 1 The spectral parameters taken from the Raman spectra of the acid-, ann- and sup-MWCNTs

Material	D-band peak position/cm^{-1}	G-band peak position/cm^{-1}	D-band intensity/ arbitrary units	G-band intensity/ arbitrary units	D-band FWHM/cm^{-1}	G-band FWHM/cm^{-1}	Ratio of I_D/I_G
Acid-MWCNTs	1,332.2	1,581.8	328.2	602.5	98	28	0.54
Ann-MWCNTs	1,332.9	1,575.8	203.5	574.8	54	25	0.35
Sup-MWCNTs	1,332.9	1,578.5	113.2	582.4	30	20	0.19

The relative errors in each value are as described in the "Materials and methods".

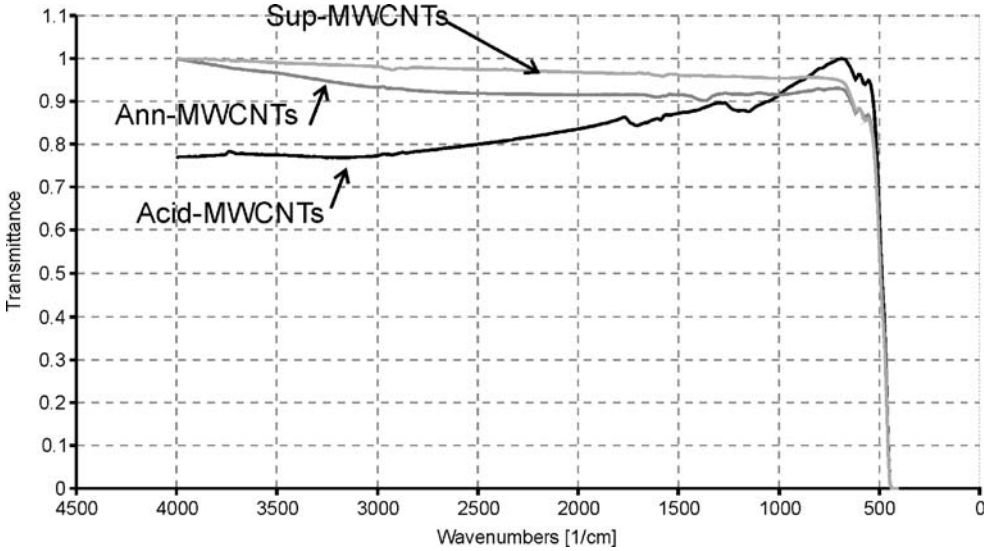

Fig. 4 Overlaid normalised FTIR spectra of the acid-, ann- and sup-MWCNTs

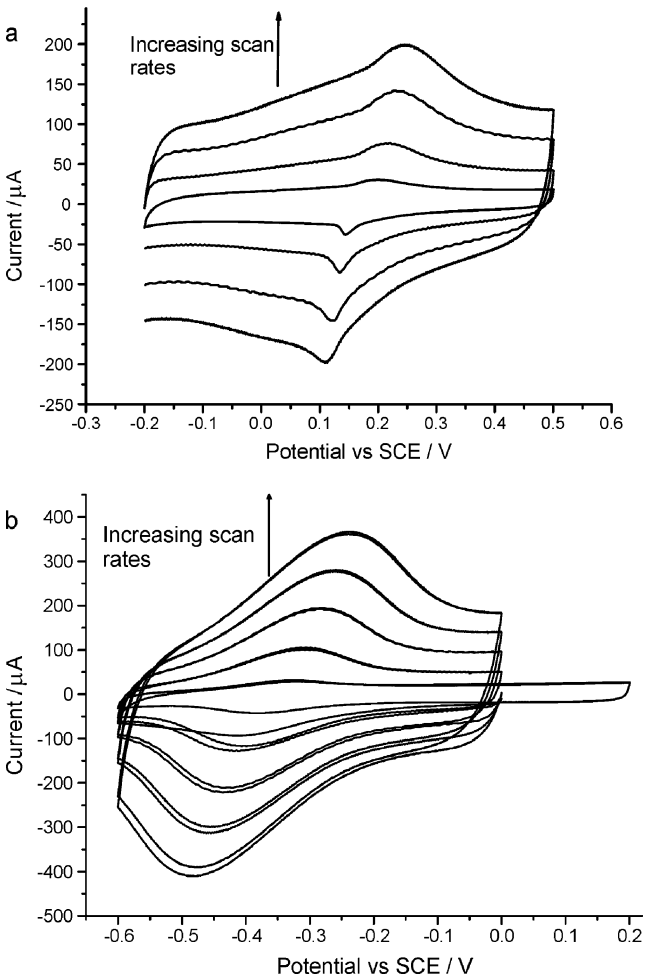

Fig. 5 The overlaid cyclic voltammograms of the acid-MWCNTs recorded at varying scan rates (10–500 mV s^{-1}) in **a** 1.0 mM $K_4Fe(CN)_6$ + 0.1 M KCl and **b** 1.0 mM $Ru(NH_3)_6Cl_3$ + 0.1 M KCl (two consecutive scans shown for each scan rate)

substitutionally labile, sufficiently so as to be considered toxic via the release of cyanide ion (CN^-) [51]. Guided by chemical intuition, we propose that some (but not all) of the ferricyanide complex formed upon oxidation may be reacting with the surface carboxyl or quinonyl groups, which decorate the edge-plane sites at which the oxidation must occur via ligand substitution. This new complex may then be either reduced back to ferrocyanide with concomitant release from the carbon surface, akin to "stripping" of the ferricyanide, whilst at the same time some of the ferricyanide ions, which remained in solution, are also reduced back to ferrocyanide in a normal diffusion-controlled process. Binding of the ferricyanide ion to the carbon surface is likely to be more prevalent at slower scan rates than at higher scan rates, reflecting the kinetics of the chemisorption process. As such, the reduction peak is much sharper and more akin to a surface-bound stripping process at lower scan rates, whilst at higher scan rates, the peak looks more like a familiar diffusion-controlled process. At small values of x, the difference between $y=mx$ and $y=mx^{1/2}$ is small (in this case y=peak current, x=scan rate). At low scan rates (up to 100 mV s^{-1}), a plot of peak current vs. scan rate is also linear (R^2=0.98), which would suggest a surface-bound species. As the voltammetry is dominated by diffusion at higher scan rates, the plot of reductive peak current vs. square root scan rate over the entire voltage scan rate is also linear, and the voltammetry then still appears to be under diffusion control. This suggests that the overall voltammetric response observed is an admixture of both small amounts of surface-bound species and the same redox species diffusing in solution.

To further investigate this, the following control experiment was performed. The acid-MWCNTs modified elec-

trode was held at +0.5 V vs. SCE for 60 s in the 1.0 mM ferrocyanide solution before being removed under potentiostatic control, gently rinsed in pure water and placed into a solution of 0.1 M KCl containing no ferrocyanide. Cyclic voltammetry was then recorded as described above and was found to be almost indistinguishable from that shown in Fig. 5a, lending further support to our hypothesis discussed above.

The voltammetric response of the acid-MWCNTs towards the hexaammineruthenium(III) redox probe also produces an unexpected response (Fig. 5b). Again, a quasireversible redox system is observed as expected, but in contrast to the voltammetry seen at the bare carbon electrodes described above, both the oxidative and reductive waves have become very broad. Whilst plots of peak current vs. the square root of voltage scan rate are linear over the entire range of scan rates studied, the voltammetric wave shape is once again indicative of some competition between surface adsorption (evidenced by the slightly more symmetrical wave shape than would be expected for a purely diffusion-controlled process) and diffusion-controlled voltammetry.

In this case, a ligand substitution process is less likely than in the case of ferricyanide as ruthenium(III), being a second-row transition metal ion, is generally more likely to be substitutionally inert than iron(III) [51]. Instead, we propose that any negatively charged, deprotonated surface carboxylate groups present on the surface interact electrostatically with the positively charged hexaammineruthenium (III/II) complexes, effectively forming ion-pairs on the surface. This adsorption process gives rise to the broad, symmetrical peak shape, whilst being superimposed on the usual diffusion-controlled voltammetric behaviour indicated by the variation of the peak current with the square root of voltage scan rate. This ion-pairing and electrostatic interaction may also explain why the mid-peak potential of the hexaammineruthenium(III/II) couple has been significantly altered from the value of −0.185 V vs. SCE recorded at all the bare carbon electrodes to a value of ca. −0.365 V vs. SCE.

The effect of the oxygen-containing surface groups on the voltammetric behaviour of MWCNTs becomes more apparent when we compare the voltammetry of the ann- with the acid-MWCNTs. Because the undecorated edge-plane sites in the ann-MWCNTs are likely to be high-energy-reactive sites on the nanotube surface, the immobilisation and recording of the voltammetric responses to either redox probe used herein were performed without delay to minimise the length of time the ann-MWCNTs were exposed to either atmospheric oxygen (during the casting process) or water (during the voltammetric experiments), both of which may react to reintroduce the surface groups removed during the annealing process [52, 53]. This was clearly achieved judging by the marked difference in the voltammetric response to ferrocyanide of the ann- (Fig. 6a) compared to the acid-MWCNTs. The voltammetric behaviour of the ann-MWCNTs is almost identical to that of a freshly polished eppg electrode, shown in Fig. 6b for comparison (again with minimal time between renewing a fresh eppg surface by polishing and recording the voltammetry to reduce the number of surface groups present on the eppg), except that the ann-MWCNTs exhibit a larger background capacitive current than the eppg due in part to the larger surface area of the ann-MWCNTs. The voltammetry of the ann-MWCNTs in the hexaammineruthenium(III) solution (not shown) is also similar to that observed at the eppg electrode apart from the increased capacitance at the ann-MWCNTs. No evidence of strong interactions with the ann-MWCNT surface is observed in this case, and the voltammetry is characteristic of a purely diffusion-controlled process, further supporting our hypothesis that the strong interactions between either redox probe and the MWCNT

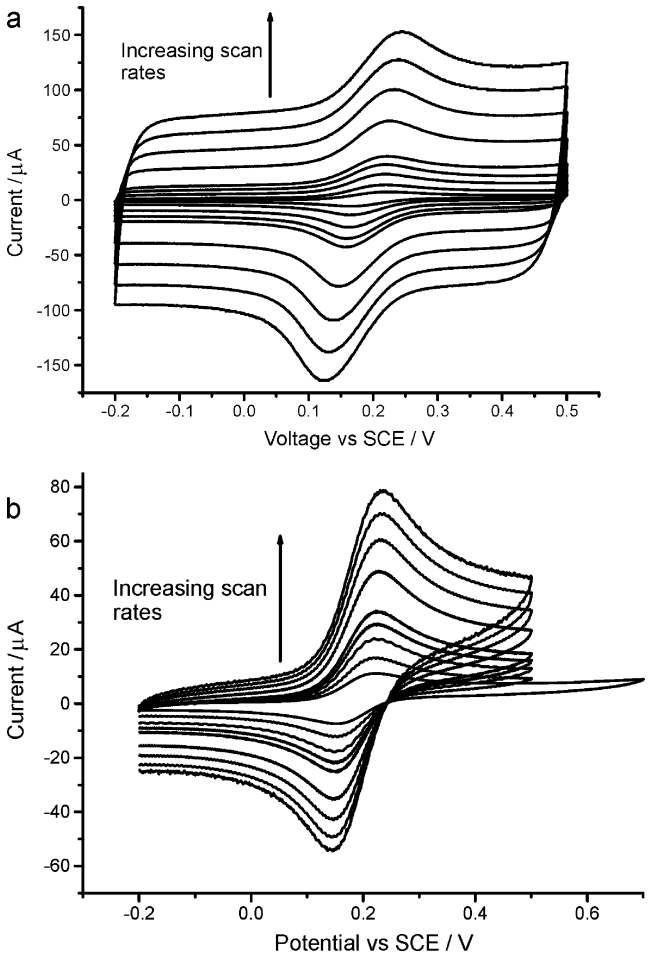

Fig. 6 The overlaid cyclic voltammograms of **a** the ann-MWCNTs and **b** a freshly prepared bare eppg electrode recorded at varying scan rates (10–500 mV s^{-1}) in 1.0 mM $K_4Fe(CN)_6$ + 0.1 M KCl

surface is dependent on the presence of the oxygen-containing surface groups.

Figure 7 shows the response of the sup-MWCNTs in ferrocyanide. The sup-MWCNTs should possess very few edge-plane defect sites as most of the tubes are closed, and the defects in the tube walls should be almost entirely removed as evidenced by the HRTEM imaging and the Raman characterisation. However, voltammetry corresponding to the quasi-reversible redox behaviour of ferrocyanide is still observed. The voltammetric behaviour is different to that of the ann-MWCNTs, which possess many edge-plane sites, with the voltammetric peaks being less pronounced above the background charging than is observed at either the ann-MWCNTs or eppg electrode. In fact, the sup-MWCNT voltammetry is remarkably similar to that previously reported for the original native arc-MWCNTs from which they were made [35]. In this case, the voltammetric wave shape exhibits some characteristics of array-like behaviour, particularly at the higher scan rates, with the peak being less pronounced and the peak becoming slightly more sigmoidal in shape [49, 50]. This has been attributed in our previous study to the presence of nanometre-sized "carbon onions", impurities in the arc-MWCNTs, which as discussed in the "Introduction" cannot be separated form the arc-MWCNTs amongst which they are randomly distributed [35]. These carbon onions have similar reactivity and properties to the MWCNTs, and hence, have remained even after the super-annealing process. They also can contain edge-plane defect sites, particularly those nanoonions formed with their graphene sheets in a "Swiss-roll-like" structure rather than as giant fullerenes [35]. Because of this Swiss-roll structure, the ends of the graphene sheets cannot be annealed and must terminate as an edge-plane site.

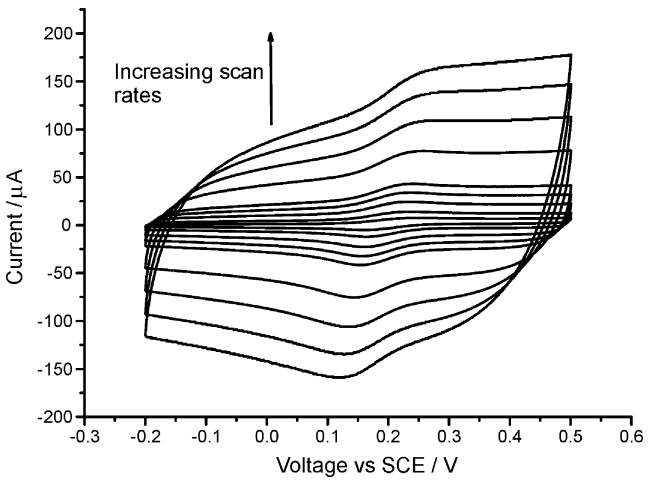

Fig. 7 The overlaid cyclic voltammetric response of the sup-MWCNTs at varying scan rates (10–500 mV s^{-1}) in 1.0 mM $K_4Fe(CN)_6$ + 0.1 M KCl

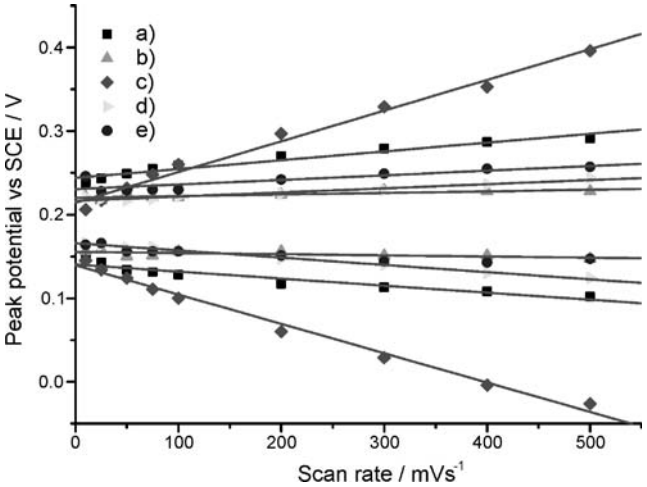

Fig. 8 A plot of the measured peak potential vs. scan rate for both the oxidative and reductive waves in 1.0 mM $K_4Fe(CN)_6$ + 0.1 M KCl recorded at *a)* a bare GC electrode, *b)* a bare eppg electrode, *c)* the acid-, *d)* the ann- and *e)* the sup-MWCNTs

Again, similar behaviour to native arc-MWCNTs was observed for the sup-MWCNTs in the hexaaminеruthenium (III) solution (not shown). Thus, we can provide voltammetric evidence that the super-annealing process has restored the MWCNTs back to their original pristine condition, voltammetrically indistinguishable from arc-MWCNTs.

Figures 8 and 9 show the variation of the peak-to-peak separation with the voltage scan rate for all the bare carbon electrodes and each type of MWCNT-modified electrode studied in ferrocyanide and hexaammineruthenium(III) solutions, respectively. The peak-to-peak separation for a truly reversible system with fast electrode kinetics under diffusion control should not vary with the scan rate

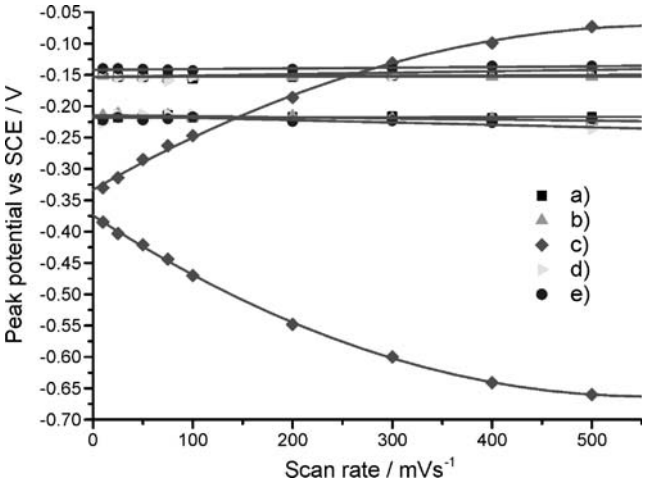

Fig. 9 A plot of the measured peak potential vs. scan rate for both the oxidative and reductive waves in 1.0 mM $Ru(NH_3)_6Cl_3$ + 0.1 M KCl recorded at *a)* a bare GC electrode, *b)* a bare eppg electrode, *c)* the acid-, *d)* the ann- and *e)* the sup-MWCNTs

[49, 50]. For systems with sluggish electrode kinetics (irreversible systems), the peak-to-peak separation rapidly increases with increasing scan rate, and the peak-to-peak separation for quasi-reversible systems increases more gradually. As such, the plots in Figs. 8 and 9 give us an insight into the different electrode kinetics between each type of electrode studied. In the case of both ferrocyanide and hexaammineruthenium(III) species, the peak-to-peak separations for the eppg, GC, ann- and sup-MWCNTs increase steadily with increasing scan rate in a similar fashion. However, the acid-MWCNTs display significantly larger increases in the peak-to-peak separation and in the case of hexaammineruthenium(III), show a dramatic shift in the mid-peak potential. Clearly, the presence of oxygen-containing surface groups has strongly inhibited the rate of electron transfer at the edge-plane defect sites that these groups decorate. Reassuringly, the ann-MWCNTs, which expose only undecorated edge-plane sites, is almost indistinguishable from the eppg electrode, further confirming that it is these sites, which are the sites for electron transfer in MWCNTs. Note that again the hexaammineruthenium(III) redox probe exhibits closer to ideal behaviour compared to the ferrocyanide. The authors advise caution when using the latter "standard" redox probe to characterise carbon electrode surfaces or voltammetric behaviour and at the very least recommend that tandem experiments be performed using the more closer to ideally behaved hexaammineruthenium(III) complex (although we have also shown that even this can, in certain circumstances, behave less than ideally). We note that these findings are in agreement with previous reports using hexaammineruthenium(III) and potassium ferrocyanide on gold electrodes [54, 55].

Finally, if we compare the background charging current at the three types of MWCNT, we see that both the ann- and the sup-MWCNTs have roughly similar values of capacitive current, ca. 175 μA at 500 mV s^{-1}. This large background current, characteristic of MWCNT voltammetry, is usually associated with the increased electroactive surface area of the MWCNTs compared to the underlying substrate upon which they are immobilised. However, the acid-MWCNTs have an even greater capacitive current of ca. 250 μA at 500 mV s^{-1}. The structure, and hence, the surface area of the acid-MWCNTs should certainly be identical to that of the ann-MWCNTs and similar even to the sup-MWCNTs. Hence, it appears that the presence of the surface groups on the acid-MWCNTs also contribute significantly to the background charging. The most likely explanation for this is that the surface carboxyl groups can become deprotonated, especially at the pH of most (unbuffered) electrolyte solutions of the simple type used herein (0.1 M KCl in pure water) and, therefore, contribute an additional negative charge to the surface of the MWCNTs, which is then balanced by the movement of counter ions from the solution into the double-layer, increasing the net capacitive charging current.

Note that the inhibition of the electron transfer at the acid-MWCNTs cannot simply be due to electrostatic "blocking" of the surface caused by negatively charged carboxylate groups repelling the ferrocyanide ion. If this were the case, then the voltammetry should resemble that seen for other examples of electrostatic blocking [56], which it does not. Furthermore, one would expect that if negatively charged surface groups decrease the apparent rate of elelctron transfer to negatively charged ions, then they would increase in the apparent rate of electron transfer to positively charged ions such as the hexaammineruthenium (III) ion, which is also not observed.

This argument is further supported by carrying out voltammetry at the acid-, ann- and sup-MWCNT-modified electrodes with a neutral redox probe, namely 1.0 mM norepinephrine in pH 5.7 acetate buffer. The pH of the buffered solution is below both the pK_a of the norepinephrine (pK_a 6.3) [57], ensuring that it is a neutral molecule, and also the pH is below that of the likely pK_a of the carboxylic acid groups on the surface of the acid-MWCNTs (pK_a 6.7) based on the work of Abiman et al. [56]. In all cases, a quasireversible wave was observed consistent with the literature [19–21]. Norepinephrine has been frequently used to explore the apparent "electrocatalyis" observed in the presence of edge-plane defects. This is typically manifested by a decrease in the overpotential required to drive the redox process in the presence of electroactive edge-plane sites [19–21]. The measured peak potentials for the oxidation of norepinephrine at each type of electrode studied are reported in Table 2. Again, the trend is in agreement with that seen using the charged redox probes in unbuffered electrolyte, with the ann-MWCNTs exhibiting the fastest rate of electron transfer (lowest peak potential required to oxidise norepinephrine), the acid-MWCNTs exhibiting much slower electron transfer due to the presence of oxygen functional groups decorating the edge-plane defects and the

Table 2 The oxidative peak potential recorded at a scan rate of 100 mV s^{-1} in 0.1 mM norepinephrine in pH 5.7 acetate buffer at each electrode studied

Electrode material	Peak potential/V vs. SCE
Glassy carbon	0.385
Bppg	No peak observed
Eppg	0.330
Acid-MWCNT	0.277
Ann-MWCNT	0.249
Sup-MWCNT	0.255

sup-MWCNTs exhibiting similar behaviour to the underlying GC electrode.

Conclusions

The role of surface functional oxygen-containing functional groups, which decorate edge-plane-like defects on MWCNTs, and the role of the edge-plane-like defects themselves have been explored by a series of modifications of the arc-MWCNT structure involving acid pre-treatment, annealing at 900 °C and super-annealing at 1,750 °C. The effect of the harsh acid pre-treatment is to introduce open tube ends and holes ion the tube walls, creating edge-plane-like defect sites and to decorate these sites with surface functional groups. After annealing at 900 °C, these surface functional groups are removed, revealing numerous undecorated edge-plane-like sites as revealed using vibrational spectroscopic techniques. Super-annealing restores the pristine MWCNT structure, removing holes and closing the ends of the nanotubes. The voltammetric response of the acid-MWCNTs towards two standard redox probes was found to be strongly affected by the surface functionality. The rate of electron transfer, by comparison of the peak-to-peak separation with a pure eppg electrode, was found to be significantly slower. Upon revealing the undecorated edge-plane-like sites in the ann-MWCNTs, the electron transfer kinetics were found to become faster (giving a more reversible voltammetric response), and the voltammetry was highly comparable to that obtained at the eppg electrode. This is further conclusive evidence to support our previous studies, which indicated that the electroactive sites on MWCNTs are located at the tube ends and edge-plane-like defects at holes in the tube walls. Super-annealing, to remove most of the edge-plane defect sites on the sup-MWCNTs, was also found to change the voltammetric response, with the observed wave shapes taking on more array-like character. The voltammetry observed at the sup-MWCNTs is identical to that of the original arc-MWCNTs where it has been shown that the voltammetric response is attributable to edge-plane defects residing on carbon nanoonion impurities randomly dispersed amongst the arc-MWCNTs with which they are formed.

The background capacitive charging currents at both the ann- and sup-MWCNTs are similar and larger than observed at either a bare GC, eppg or bppg electrode; this simply reflects the greater surface area of these materials. However, the acid-MWCNTs show much larger background capacitive currents as the surface functional groups, particularly deprotonated carboxyl groups also contribute to the charge contained in the double-layer surrounding the acid-MWCNTs on the electrode surface.

Finally, we have shown that there are strong interactions between both standard redox probes, ferrocyanide and hexaaminеruthenium(III) and oxygen-containing surface groups on MWCNTs. As such, we recommend caution in using these redox probes to characterise carbon and in particular, MWCNT surfaces.

Acknowledgment GGW thanks St John's College, Oxford for a Junior Research Fellowship.

References

1. Monthioux M, Kuznetsov VL (2006) Carbon 44:1621
2. Oberlin A, Endo M (1976) J Cryst Growth 32:335
3. Wiles PG, Abrahamson J (1978) Carbon 16:341
4. Iijima S (1991) Nature 354:56
5. http://www.nano-lab.com/
6. Wildgoose GG, Banks CE, Leventis HC, Compton RG (2006) Microchim Acta 152:187
7. Leonhardt R, Ritschel M, Bartsch K, Graff A, Taschner C, Fink J (2001) J Physique IV: Proc 11:Pr3/445
8. Wang YY, Tang GY, Koeck FAM, Brown B, Garguilo JM, Nemanich RJ (2004) Diamond Rel Mater 13:1287
9. Ebbesen TW (1994) NATO ASI Ser C 443:11
10. Kratschmer W, Lamb LD, Fostiropoulos K, Huffman DR (1990) Nature 347:354
11. Liu C, Cong HT, Li F, Tan PH, Cheng HM, Lu K, Zhou BL (1999) Carbon 37:1865
12. Dai X, Wildgoose GG, Compton RG (2006) Analyst 131:901
13. Kruusma J, Mould N, Jurkschat K, Crossley A, Banks CE (2007) Electrochem Commun 9:2330
14. Jones CP, Jurkschat K, Crossley A, Compton RG, Riehl BL, Banks CE (2007) Langmuir 23:9501
15. Jurkschat K, Ji X, Crossley A, Compton RG, Banks CE (2007) Analyst 132:21
16. Sljukic B, Banks CE, Compton RG (2006) Nano Lett 6:1556
17. Banks CE, Crossley A, Salter C, Wilkins SJ, Compton RG (2006) Angew Chem Int Ed 45:2533
18. Batchelor-McAuley C, Wildgoose GG, Compton RG, Shao L, Green MLH (2008) Sens Act B. DOI 10.1016/j.snb.2008.01.049
19. Banks CE, Compton RG (2005) Anal Sci 21:1263
20. Banks CE, Compton RG (2006) Analyst 131:15
21. Banks CE, Davies TJ, Wildgoose GG, Compton RG (2005) Chem Commun 7:829
22. Thorogood CA, Wildgoose GG, Crossley A, Jacobs RMJ, Jones JH, Compton RG (2007) Chem Mater 19:4964
23. Masheter AT, Xiao L, Wildgoose GG, Crossley A, Jones JH, Compton RG (2007) J Mater Chem 17:3515
24. Thorogood CA, Wildgoose GG, Jones JH, Compton RG (2007) New J Chem 31:958
25. Dumitrescu I, Wilson NR, Macpherson JV (2007) J Phys Chem C 111:12944
26. Du Vall S, Yang H-H, McCreery RL (1999) Proc Electrochem Soc 99-5:33
27. McCreery RL, Cline KK, McDermott CA, McDermott MT (1994) Coll Surf A 93:211
28. Cline KK, McDermott MT, McCreery RL (1994) J Phys Chem 98:5314
29. McDermott CA, Kneten KR, McCreery RL (1993) J Electrochem Soc 140:2593
30. Ranganathan S, Kuo T-C, McCreery RL (1999) Anal Chem 71:3574
31. Chou A, Boecking T, Singh NK, Gooding JJ (2005) Chem Commun 7:842

32. Banks CE, Ji X, Crossley A, Compton RG (2006) Electroanalysis 18:2137
33. Ji X, Banks CE, Crossley A, Compton RG (2006) ChemPhysChem 7:1337
34. Liu J, Chou A, Rahmat W, Paddon-Row MN, Gooding JJ (2005) Electroanalysis 17:38
35. Henstridge MC, Shao L, Wildgoose GG, Compton RG, Tobias G, Green MLH (2008) Electroanalysis 20:498
36. Liu J, Rinzler AG, Dai H, Hafner JH, Bradley RK, Boul PJ, Lu A, Iverson T, Shelimov K, Huffman CB, Rodriguez-Macias F, Shon Y-S, Lee TR, Colbert DT, Smalley RE (1998) Science 280:1253
37. Kuznetsova A, Mawhinney DB, Naumenko V, Yates JT, Liu J, Smalley RE (2000) Chem Phys Lett 321:292
38. Yudasaka M, Ichihashi T, Kasuya D, Kataura H, Iijima S (2003) Carbon 41:1273
39. Bougrine A, Dupont-Pavlovsky N, Naji A, Ghanbaja J, Mareche JF, Billaud D (2001) Carbon 39:685
40. Brown SDM, Corio P, Marucci A, Dresselhaus MS, Pimenta MA, Kneip K (2000) Phys Rev B 61:R5137
41. Delhaes P, Couzi M, Trinquecoste M, Dentzer J, Hamidou H, Vix-Guterl C (2006) Carbon 44:3005
42. Paillet M, Michel T, Meyer JC, Popov VN, Henrard L, Roth S, Sauvajol J-L (2006) Phys Rev Lett 96:257401
43. Shanmugan S, Gedanken A (2006) J Phys Chem B 110:2037
44. Sveningsson M, Morjan R-E, Nerushev OA, Sato Y, Bäckström J, Campbell EEB, Rohmund F (2001) Appl Phys A 73:409
45. Vix-Guterl C, Couzi M, Dentzer J, Trinquecoste M, Delhaes P (2004) J Phys Chem B 106:19361
46. Wang YY, Tang GY, Koeck FAM, Brown B, Garguilo JM, Nemanich RJ (2004) Diamond Rel Mater 13:1287
47. Tuinistra F, Koenig JL (1970) J Chem Phys 53:1126
48. Masheter AT, Abiman P, Wildgoose GG, Wong E, Xiao L, Rees NV, Taylor R, Attard GA, Baron R, Crossley A, Jones JH, Compton RG (2007) J Mater Chem 17:2616
49. Compton RG, Banks CE (2007) Understanding voltammetry. World Scientific, Singapore
50. Bard AJ, Faulkner LR (2001) Electrochemical methods fundamentals and applications. Wiley, New York
51. Greenwood NN, Earnshaw A (1984) Chemistry of the elements. Pergamon, London
52. Sendt K, Haynes BS (2007) J Phys Chem C 111:5465
53. Zhu Z, Lu GQ, Finnerty J, Yang RT (2003) Carbon 41:635
54. Diao P, Guo M, Hou Q, Xiang M, Zhang Q (2006) J Phys Chem B 110:20386
55. Sabatani E, Rubinstein I (1987) J Phys Chem 91:6663
56. Abiman P, Crossley A, Wildgoose GG, Jones JH, Compton RG (2007) Langmuir 23:7847
57. Kenakin TP (1981) J Pharm Experiment Therap 216:210